CrystEngComm

Dynamic Article Links ►

2013, DOI: 10.1039/c3ce40859k.

PAPER

Progressive Decoration of Pentanuclear Cu(II) 12-Metallacrown-4 Nodes Towards Targeted 1- and 2D Extended Networks‡

Cecelia McDonald,[a] Teresa Whyte,[a] Stephanie M. Taylor,[c] Sergio Sanz,[c] Euan. K. Brechin,[c] Declan Gaynor[b]* and Leigh F. Jones[a]*

Received (in XXX, XXX) Xth XXXXXXXXX 20XX, Accepted Xth XXXXXXXXX 20XX
DOI: 10.1039/b000000x

The synthesis, structures and magnetic characterisation of a family of discrete planar pentanuclear Cu(II) 12-MC-4 metallacrowns of formulae $[Cu_5(L_1)_4(MeOH)_4](ClO_4)_2$ (**1**), $[Cu_5(L_1)_4(py)_2](ClO_4)_2 \cdot py$ (**2**), $[Cu_5(L_1)_4(py)_6](ClO_4)_2$ (**3**) and $[Cu_5(L_2)_4(MeOH)_4](ClO_4)_2.H_2O$ (**7**) (where L_1H_2 = 2-(dimethylamino)phenylhydroxamic acid and L_2H_2 = 2-(amino)phenylhydroxamic acid) are reported. UV-vis and Electrospray MS studies indicate solution stability with respect to their $\{Cu_5(L)_4\}^{2+}$ cores. Magnetic susceptibility measurements confirm strong antiferromagnetic exchange between the Cu(II) ions resulting in isolated $S = ½$ ground spin states. The introduction of ditopic co-ligands such as 4,4'-bipyridine (4,4'-bipy), pyrazine (pz) and 4,4-azopyridine (4.4-azp) results in their coordination at a number of axial Cu(II) sites within the $\{Cu_5\}$ metallacrown nodes to afford the extended networks $\{[Cu_5(L_1)_4(4,4'\text{-bipy})_3](ClO_4)_2(H_2O)\}_n$ (**4**), $\{[Cu_5(L_1)_4(4,4\text{-azp})_2(MeOH)_2].(ClO_4)_2\}_n$ (**5**) and $\{[Cu_5(L_2)_4(pz)_2(MeOH)_3](ClO_4)_2.MeOH\}_n$ (**6**).

Introduction

Interest in investigating the coordination chemistry of hydroxamic acids lies in their pertinence to the field of biology and their ability to act as selective inhibitors of histone deacetylase, urease and matrix metalloproteinase enzymes, to name but a few,[1] leading to therapeutic applications as anti-fungal, anti-tuberculosis, anti-osteoarthritis, anti-hypertension and anti-cancer agents.[2] One such ligand at the forefront of our research is 2-(dimethylamino)phenylhydroxamic acid (L_1H_2 in Scheme 1). Previous studies using this ligand have produced some interesting results which include an heptanuclear $[Ni_7]$ complex comprising a ferrimagnetic ground state and unique hydroxamate ligand binding modes[3] and more pertinently to this work, a clam-shaped dimer of $[Cu(II)_5]$ 12-MC-4 metallacrowns,[4] a family of metallomacrocycles first synthesised and categorised by Pecoraro *et al*.[5] Since this discovery an ever growing number of metallacrowns comprising many different metal ions (Cu(II), Mn(II/III), Fe(III), Co(II), Ni(II), Ln(III) *etc*) with numerous topologies (currently ranging from 9-MC-3 to an impressive 60-MC-20) have been reported using a myriad of organic bridging ligands to achieve them.[5] Furthermore these aesthetically pleasing complexes have regularly shown to be viable target molecules due to their solution stablility, selective cation and anion binding, ligand exchange capabilities and in their use as building blocks towards extended architectures. As a result such moieties have applications in fields such as catalysis,[6] molecular recognition,[7] selective substrate sorption,[8] and luminescent[9] and magnetic materials.[10]

With these thoughts in mind we describe here the use of L_1H_2 and its analogue 2-(amino)phenylhydroxamic acid (L_2H_2) to form an extended family of 12-$MC_{Cu(II)}$-4 $[Cu(II)_5]$ metallacrowns whose terminal ligands may be exchanged in a controlled and progressive manner ultimately towards the self-assembly of 1- and 2D extended networks comprising $[Cu(II)_5]$ nodes. These are the first to be formed using pyridyl connector ligands and are extremely rare examples of $[Cu_5]$ metallacrown coordination polymers.

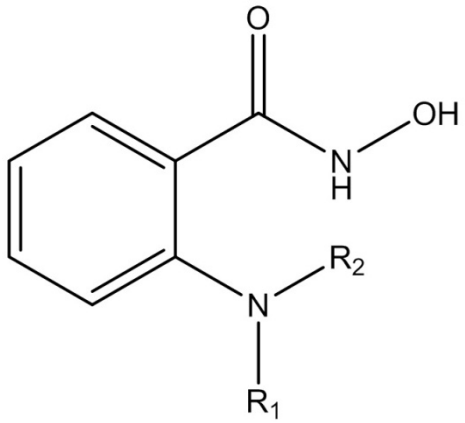

Scheme 1 Schematic of the hydroxamic acid ligands used in this work ($R_1 = R_2$ = Me; L_1H_2) ($R_1 = R_2$ = H; L_2H_2).

Results and Discussion

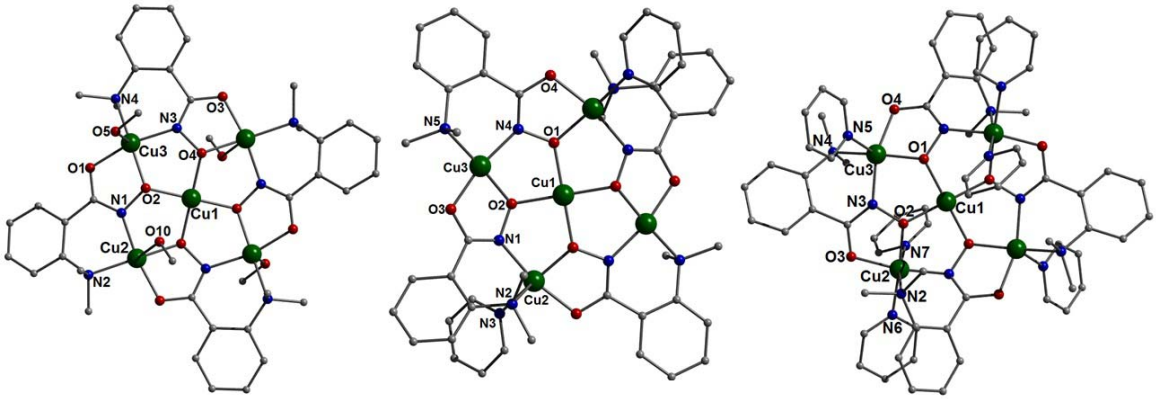

Figure 1 Crystal structures of the [Cu_5] metallacrown cations of **1-3 (**left→right) as viewed perpendicular to their {Cu_5} planes. Colour code: Green (Cu), Red (O), Blue (N), Carbon (C). This colour code is used throughout this work. Hydrogen atoms and perchlorate counter ions have been omitted for clarity.

The methanolic reaction of $Cu(ClO_4)_2.6H_2O$, 2-(dimethylamino)phenylhydroxamic acid (L_1H_2) and NaOH gives a dark green solution from which crystals of the pentanuclear metallacrown $[Cu_5(L_1)_4(MeOH)_4](ClO_4)_2$ (**1**) are obtained upon slow evaporation of the mother liquor in ~10% yield (monoclinic *C2/c* space group). † For full crystallographic data see Tables 1 (**1-4**) and 2 (**5-7**). The structure in **1** possesses a planar core which comprises a central distorted square planar Cu(II) ion (Cu1) surrounded by four five-coordinate Cu(II) centres (Cu2-Cu3 and symmetry equivalents (s.e)), each exhibiting almost idealised square-based pyramidal geometries (τ = 0.004 for Cu2, τ = 0.07 for Cu3).[11] The four 2-(dimethylamino)phenylhydroxamic acid ligands are doubly deprotonated (L_1^{2-}) and bridge the outer Cu(II) ions (Cu2 and Cu3) using the η^1: η^1: η^2: η^1, μ_3-bonding motif (Fig. 1, left). The four Cu-O bonds stabilising the central Cu1 are provided by the ligand oxime group O atoms O2 and O4 (Cu1-O2 = 1.892 Å, Cu1-O4 = 1.896 Å), while their oximic N atoms (N1 and N3) bond to the peripheral Cu2 and Cu3 ions (Cu2-N1 = 1.913 Å, Cu3-N3 = 1.933 Å). The fifth (axial) coordination sites on the outer Cu ions are each occupied by MeOH ligands at distances of 2.558 Å (Cu2-O10) and 2.303 Å (Cu3-O5). The $\{Cu(II)_5(L_1)_4(MeOH)\}^{2+}$ cations in **1** are charge balanced by two ClO_4^- counter anions sitting above and below the planar {Cu_5} arrays, which also partake in inter-molecular H-bonding with the aforementioned terminal MeOH ligands (O10(H10)···O9 = 2.235 Å; Fig. 2). These H-bonds link the individual {Cu_5} units together, resulting in the formation of zig-zag rows that propagate along the *c* direction of the unit cell. These separate rows then arrange along *a* with alternating wave-like phases (Fig. 3).

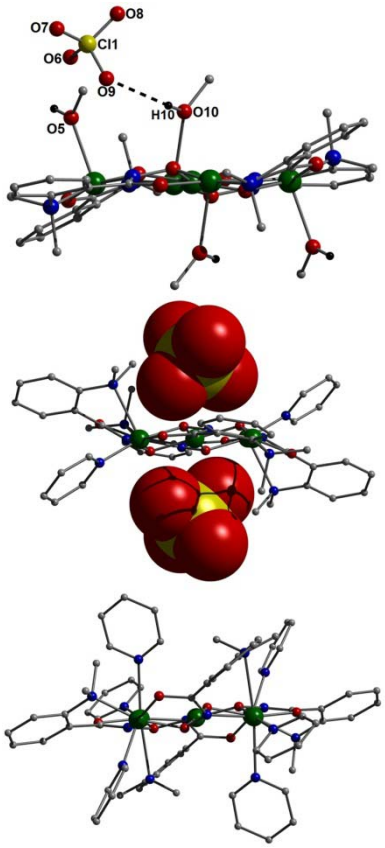

Figure 2 Crystal structures of **1** (top), **2** (middle) and **3** (bottom) as viewed parallel to their planar {Cu_5} cores. The ClO_4^- counter anions in **2** are represented in space-fill mode. The peripheral ClO_4^- anions in **3** have been omitted.

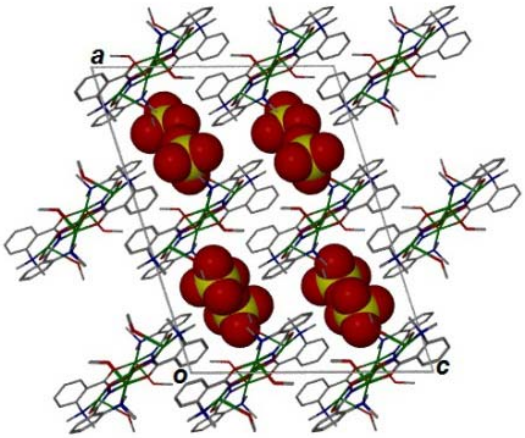

Figure 3 Crystal packing in **1** as viewed along the *a* axis of the unit cell. The perchlorate counter anions are space-fill represented. Hydrogen atoms have been omitted for clarity.

Examination of the molecular structure of the cation of **1** revealed several opportunities for exploitation, by taking advantage of the coordinative flexibility of the Cu(II) ion, the vacant coordination sites on some of the Cu ions, and the potential for substituting the terminally bound alcohols on Cu2 and Cu3. Addition of 1 cm^3 (12.4 mmol) of pyridine to the experimental procedure employed in the production of **1** led to the formation of the analogous metallacrown $[Cu_5(L_1)_4(py)_2](ClO_4)_2{\cdot}py$ (**2**) (Fig. 1, middle). Complex **2** crystallises in the triclinic *P*-1 space group in ~15% yield. The core in **2** closely resembles that of **1**, however it differs in two significant ways. Firstly the central Cu(II) ion (Cu1) once again possesses four equatorial Cu-O_{oxime} bonds (Cu1-O1 = 1.915 Å, Cu1-O2 = 1.933 Å) but also exhibits two long axial close contacts with the two symmetry equivalent, charge balancing, ClO_4^- anions (Cu1-O5 = 2.681 Å), which sit above and below the distorted $\{Cu_5\}$ core, respectively. The second major difference is the puckering of the $\{Cu_5\}$ core in **2** compared to that of **1**, as highlighted in Figure 2 (middle). This is due to the presence of the two terminally bonded pyridine ligands attached to Cu2 (and s.e.) (Cu2-N3 = 2.006 Å). More interestingly, although the additional (or addition of) pyridine in **2** does not alter the distorted square-based pyramidal coordination geometry of Cu2 and its symmetry equivalents (τ = 0.024),[11] the pyridine ligands force the hydroxamate ligands (L_1^{2-}) to distort away from the $\{Cu_5\}$ plane. This results in the ligands -NMe_2 moiety forming a Cu-N bond at the axial position at a distance of Cu2-N2 = 2.438 Å. The Cu3 (and s.e) ion is distorted square planar in **2** (unlike in **1**) presumably due to the steric constraints enforced by the nearby ClO_4^- anions. Indeed the perchlorate O5 atom lies at a distance of 2.861 Å from Cu3, which would represent a fifth close contact around this metal ion. The $\{Cu_5\}$ moieties in **2** form rows along the *a* axis with a large inter-cluster separation of ~11.2 Å (Cu1···Cu1'). These individual rows are linked by $\pi_{centroid}\cdots\pi_{centroid}$ stacking of their terminal and symmetry equivalent pyridine ligands (C10-C14-N3] ···[C10′-C14′-N3′] = 3.644 Å). These individual rows then pack in the common brickwork motif and the 3D connectivity in **2** is completed *via* H-bonding through the ClO_4^- anions and pyridine molecules of crystallisation (Cl1(O6)···(H33)C33 = 2.673 Å and Cl1(O8)···(H13)C13 = 2.508 Å; Fig. S1).

An even greater excess of pyridine (5 cm^3; 62.0 mmol) is added to the procedure used to make complex **1** more of the Cu(II) sites become occupied, forming the metallacrown $[Cu_5(L_1)_4(py)_6](ClO_4)_2$ (**3**) (Fig 1, right and Fig. 2, bottom). The formation of this analogue merely takes advantage of the coordinatively unsaturated Cu(II) centres. On close scrutiny of the crystal structures of **2** and **3** several structural differences become apparent. Firstly the introduction of the extra pyridine ligands has pushed the ClO_4^- counter anions away from the primary coordination sphere of the Cu(II) ions, rendering the central Cu1 ion (distorted) square planar in geometry. More specifically the ClO_4^- anions are located approximately 5 Å from the planar $\{Cu_5\}$ core, held in position through numerous H-bonds with aromatic and aliphatic ligand protons of all four near neighbour complexes (*e.g.* C32(H32)···O5 = 2.698 Å; C21(H21)···O6 = 2.661 Å; C9(H9C)···O7 = 2.452 Å; C12(H12)···O8 = 2.554 Å). Furthermore the outer ring Cu2 centres in **3** are now distorted octahedral in geometry (*cf.* square-based pyramidal in **2**), with elongated axial bonds forged by one pyridine ligand (N7) and one –NMe_2 group (N2) at distances of Cu2-N7 = 2.532 Å and Cu2-N2 = 2.666 Å. The bonding at Cu3 (and s.e.) is also different to that in **2**. Cu3 exhibits distorted square-based pyramidal geometry with the axial bond being to a pyridine ligand (Cu3-N5 = 2.211 Å) (τ = 0.11).[11] The individual $\{Cu_5\}$ units in **3** are connected in all directions via numerous intermolecular interactions involving the perchlorate counter anions. Each of their O atoms (O5-O8 and s.e.) partake in H-bonding interactions with either aromatic (H12, H21) or aliphatic (H8B, H9C) protons belonging to nearby L_1^{2-} or terminal pyridine ligands (C8(H8B)···O5 = 2.589 Å; C21(H21)···O6 = 2.661 Å; C9(H9C)···O7 = 2.452 Å and C12(H12)···O8 = 2.554 Å) (Fig. S2).

The retainment of the 12-MC-4 $[Cu_5]$ core upon addition of pyridine to give products **2** and **3** was by no means an entirely expected event; for example, addition of pyridine to the complex $[Cu_5(picha)_4](NO_3)_2$ (where picha = 2-picolinehydroxamic acid) resulted in a change in topology from $[Cu_5]$ to $[Cu_3]$.[12]

Table 1 Crystallographic data for complexes **1-4**

	1	**2**	**3**	**4**
Formula[a]	$C_{40}H_{56}N_8O_{20}Cl_2Cu_5$	$C_{51}H_{55}N_{11}O_{16}Cl_2Cu_5$	$C_{66}H_{70}N_{14}O_{16}Cl_2Cu_5$	$C_{66}H_{64}N_{14}O_{17}Cl_2Cu_5$
M_W	1357.53	1466.66	1703.96	1713.91
Crystal System	Monoclinic	Triclinic	Triclinic	Triclinic
Space group	C2/c	P-1	P-1	P-1
a/Å	17.9896(7)	11.283(2)	11.3067(3)	11.3776(7)
b/Å	12.2939(4)	11.482(2)	12.7372(5)	12.6211(9)
c/Å	23.8922(9)	13.688(3)	13.2511(4)	12.6793(8)
α/°	90	72.42(3)	97.753(3)	90.229(6)
β/°	107.805(4)	80.58(3)	104.985(3)	107.558(6)
γ/°	90	61.80(3)	103.130(3)	104.589(6)
V/Å^3	5031.0(3)	1489.4(5)	1762.79(10)	1673.60(19)
Z	4	1	1	1
T/K	150(2)	150(2)	150(2)	150(2)
λ[b]/Å	0.7107	0.7107	0.7107	0.7107
D_c/g cm^{-3}	1.792	1.635	1.605	1.701
μ(Mo-Ka)/ mm^{-1}	2.271	1.921	1.637	1.726
Meas./indep.(R_{int}) refl.	4607/3722 (0.0401)	5443/4757 (0.0162)	6450/5592 (0.0185)	6117/4231 (0.0867)
wR2 (all data)	0.0910	0.1152	0.0681	0.2254
$R1$[d,e]	0.0423	0.0378	0.0267	0.0696
Goodness of fit on F^2	1.074	1.074	1.063	1.023

[a] Includes guest molecules.[b] Mo-Kα radiation, graphite monochromator. [c] $wR2= [\Sigma w(|F_o^2| - |F_c^2|)^2 / \Sigma w|F_o^2|^2]^{1/2}$. [d]For observed data. [e] $R1= \Sigma||F_o| - |F_c|| / \Sigma|F_o|$.

This initial success in manipulating the primary coordination spheres of the Cu(II) centres in **1** suggested that the self assembly of a larger extended architecture could be achieved in a simple one pot reaction through addition of a linear linker ligand. This was realised upon introduction of the ditopic ligand 4,4'-bipyridine (4,4'-bipy), affording the 2D coordination polymer $\{[Cu_5(L_1)_4(4,4'\text{-bipy})_3](ClO_4)_2 \cdot H_2O\}_n$ (**4**, Figure 4). Complex **4** joins a very small group of extended networks comprising $\{Cu_5\}$ metallacrown nodes and is the first to be built using pyridyl connector ligands. Indeed previously reported examples of such architectures comprise carboxylate-based or alkali metal linker moieties and whose $\{Cu_5\}$ nodes possess different internal bridging ligands to that present in **4**.[8,13] It should be noted that the integration of structurally related metallocyclic complexes into extended network materials is also known in the literature and includes two examples containing connector pyridyl ligands.[5,14]

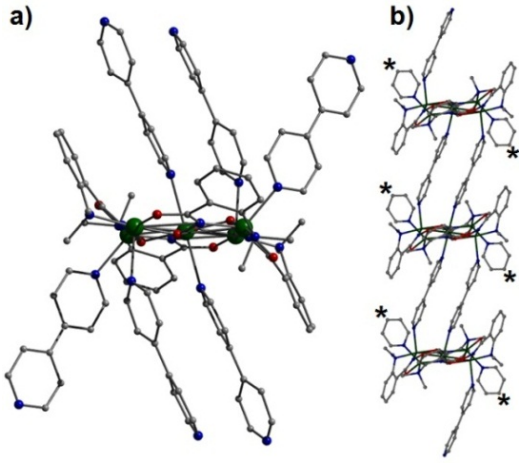

Figure 4 (a) Crystal structure of one $\{Cu_5\}$ node within the extended network **4**. (b) Structure of three $\{Cu_5\}$ nodes linked into 1D arrays by 4,4'-bipy connector ligands. The symbol ✱ highlights the points at which the 1D rows are connected (*via* 4,4'-bipy ligands) to form the 2D sheets in **4**. H-atoms, counter anions and solvent molecules have been omitted for clarity.

The extended architecture in **4** comprises rows of $\{Cu_5\}$ moieties propagating along the *a* cell direction and are connected by two ditopic 4,4'-bipy ligands. These are axially bonded to the central Cu(II) ions (Cu1 and s.e.) at N4 and the outer Cu2 ions (N3) respectively, with rather long bond lengths of Cu1-N4 = 2.495 Å and Cu2-N3 = 2.294 Å. A third dipyridyl ligand in **4** acts as a connector in between these 1D chains to form covalent 2D sheets, giving rise to a [4,4] grid topology (Figures 4 and 5). These 2D nets stack in parallel staggered layers along the *b* direction of the unit cell with an internodal distance of 12.62 Å (Cu1···Cu1′). The ClO_4^- counter anions connect the separate 2D sheets in **4** and are held in position through H-bonding with aromatic protons of nearby 4,4'-bipy (H20, H33) and L_1^{2-} ligands (H14) with distances of C20(H20)···O7 = 2.359 Å; C33(H33)···O8 = 2.397 Å and C14(H14)···O5 = 2.614 Å (Fig, 6). A water of crystallisation is also present within these 2D planes and was modelled isotropically as disordered over two sites (50:50 occupancy).

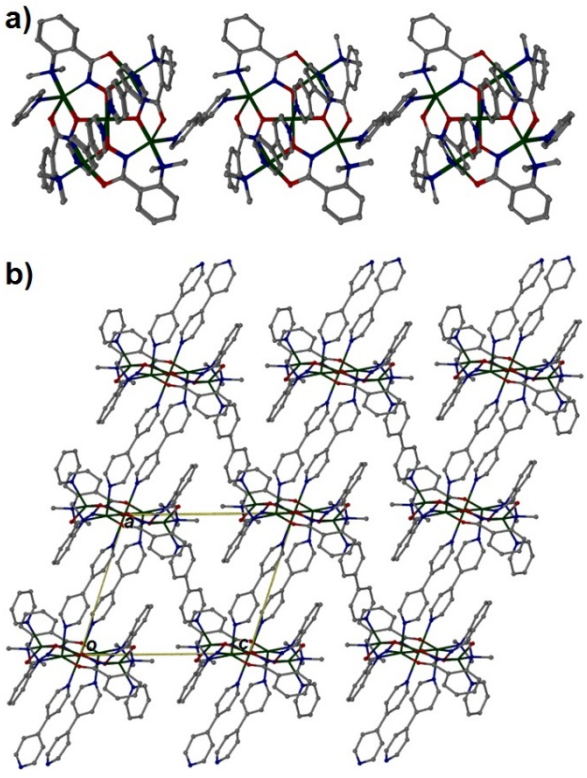

Figure 5 Birds eye (a) and perpendicular (b) views of a single 2D sheet of $\{Cu_5\}$ nodes linked into the [4,4] grid array in **4**. H-atoms, counter anions and solvent molecules have been omitted for clarity.

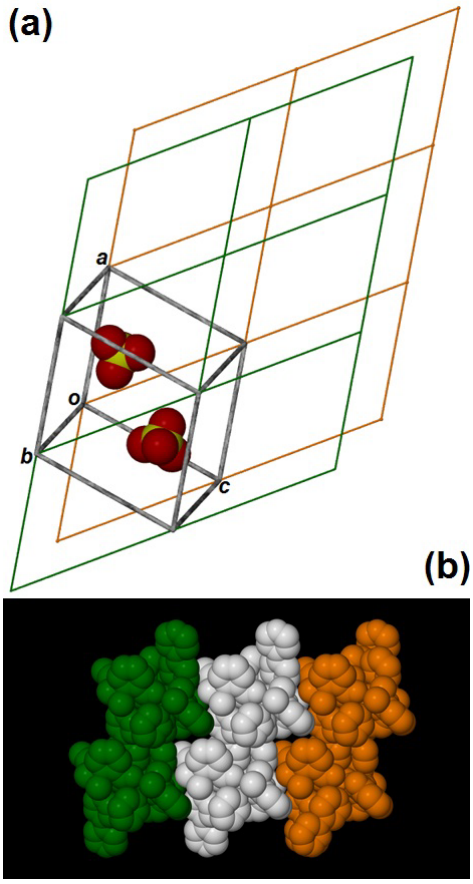

Figure 6 (a) Schematic diagram (obtained from crystal data) showing two parallel 2D grid-like sheets in **4** represented as different colours for clarity (green and orange). Each node represents one $\{Cu_5\}$ building block in **4** (taken as the central Cu1 ion). The unit cell location and its contents (ClO_4^- anions) are also shown. (b) Three colour coded 2D sheets of **4** standing parallel to one another along the *b* cell direction.

The introduction of the ditopic ligand 4,4-azopyridine (4.4-azp) to the reaction used in producing the 2D net **4** gives rise to a 1D coordination polymer of formula $\{[Cu_5(L_1)_4(4,4\text{-azp})_2(MeOH)_2](ClO_4)_2\}_n$ (**5**). Complex **5** crystallises in the monoclinic $P2_1/n$ space group (Z = 2) in ~12% yield (Fig. 7a). This change in connectivity (1D (**5**) *vs.* 2D (**4**)) is presumably due to the -N=N- bridges of the 4,4-azopyridine ligands (bonding to Cu2 and symmetry equivalents; Cu2-N5 = 2.277 Å), which show *trans* conformations in the crystal structure, leading to a zig-zag chain topology. The chains in **5** stack on top of one another in an off-set manner along the *ab* plane of the cell (Fig. 7a). Furthermore the individual chains in **5** alternate in their running direction (along *a* vs. along *b*) as we look along the *c* direction of the cell, thus lying approximately perpendicular to one another (Fig. 7b).

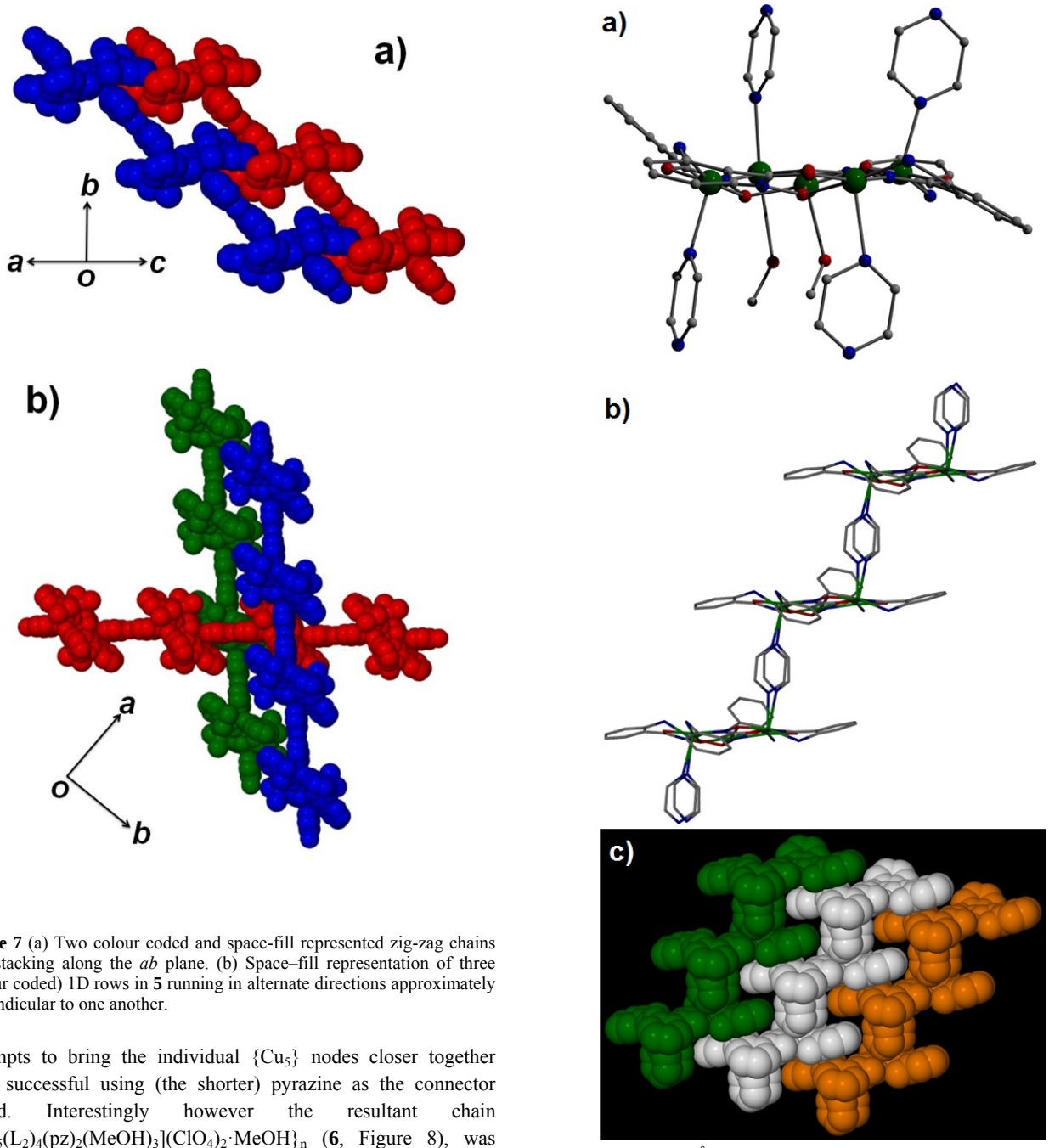

Figure 7 (a) Two colour coded and space-fill represented zig-zag chains in **5** stacking along the *ab* plane. (b) Space–fill representation of three (colour coded) 1D rows in **5** running in alternate directions approximately perpendicular to one another.

Attempts to bring the individual $\{Cu_5\}$ nodes closer together were successful using (the shorter) pyrazine as the connector ligand. Interestingly however the resultant chain $\{[Cu_5(L_2)_4(pz)_2(MeOH)_3](ClO_4)_2{\cdot}MeOH\}_n$ (**6**, Figure 8), was only produced using the ligand 2-(amino)phenylhydroxamic acid (L_2H_2; Scheme 1). No crystalline or isolable products were obtained when using 2-(dimethylamino)phenylhydroxamic acid (L_1H_2). This is presumably down to simple sterics and the bulky –NMe_2 and less bulky –NH_2 moieties in L_1H_2 and L_2H_2, respectivelyEach of the four outer Cu(II) centres (Cu2-5) are bound to one pyrazine ligand (N9-N12) which propagate the 1D rows and results in a step-like topology (Fig. 8b). The 1D rows develop along the *a* direction of the cell, while the individual rows stack in parallel inter-digitated layers along the *c* axis and are held in place by intermolecular interactions (N6(H6B)···[C9-C14]$_{centroid}$ = 3.801 Å), as observed in the 1D network in **5**. The resultant H-bonded 2D sheets stack in parallel layers along the *b* cell direction (Fig. S3). The $\{Cu_5\}$ nodes in **6** lie at an average distance of 9.396 Å (Cu1···Cu1′) which represents a significant reduction compared to **4** (12.62 Å) and **5** (13.51 Å).

Table 2: Crystallographic data for complexes **5** -**7**

	5	**6**	**7**
Formula[a]	$C_{48}H_{56}N_{12}O_{18}Cl_2Cu_5$	$C_{40}H_{47}N_{12}O_{20}Cl_2Cu_5$	$C_{32}H_{40}N_8O_{21}Cu_5$
M_W	1477.65	1404.50	1261.32
Crystal System	Monoclinic	Monoclinic	Triclinic
Space group	$P2_1/n$	$P2_1$	P-1
a/Å	12.6809(3)	9.396(2)	11.0640(3)
b/Å	10.7919(3)	26.777(5)	12.2750(4)
c/Å	20.7122(5)	10.690(2)	17.2399(6)
α/°	90	90	110.321(3)
β/°	100.018(2)	100.54(3)	96.075(3)
γ/°	90	90	96.316(2)
V/Å^3	2791.27(12)	2644.2(9)	2156.10(12)
Z	2	2	2
T/K	150(2)	150(2)	150(2)
λ[b]/Å	0.7107	0.7107	0.7107
D_c/g cm^{-3}	1.758	1.764	1.943
μ(Mo-Ka)/ mm^{-1}	2.054	2.166	2.643
Meas./indep. (R_{int}) refl.	5090 / 3963 (0.0547)	7736 / 5930 (0.0694)	7876 / 6482 (0.0262)
wR2 (all data)	0.0874	0.0758	0.0795
$R1$[d,e]	0.0379	0.0482	0.0322
G.O.F on F^2	1.025	0.963	1.063

[a] Includes guest molecules.[b] Mo-Kα radiation, graphite monochromator. [c] $wR2 = [\Sigma w(|F_o^2| - |F_c^2|)^2 / \Sigma w|F_o^2|^2]^{1/2}$. [d]For observed data. [e] $R1 = \Sigma||F_o| - |F_c|| / \Sigma|F_o|$.

Figure 8 (a) Crystal structure of one $\{Cu_5\}$ node in **6** and (b) as part of a 1D coordination polymer. (c) Space-fill representation of three colour coded step-like chains in **6**. H-atoms, counter anions and solvent molecules have been omitted for clarity.

In order to probe further the less bulky nature of the 2-(amino)phenylhydroxamate ligand (L_2^{2-}) and its contribution to producing less puckered $[Cu_5]$ metallacrowns, we decided to synthesise a discrete $[Cu_5]$ metallacrown in the form of the complex $[Cu_5(L_2)_4(MeOH)_4](ClO_4)_2.H_2O$ (**7**). The result is the crystallisation of two $\{Cu_5\}$ units within the asymmetric unit in **7** (labelled Cu1-3 and Cu4-6, respectively), which lie in close proximity to one another (Fig. S4b). Numerous intermolecular interactions are observed between them, involving aromatic and aliphatic hydroxamate protons and oxygen atoms of juxtaposed C-O groups, MeOH and ClO_4^- species. For example, the interstitial MeOH solvent of crystallisation in **7** lies in between the two unique $\{Cu_5\}$ units and its -OH group simultaneously H-bonds (*via* O20A and H20A) to an -NH_2 proton (H7A) and a carbonyl O atom (O1) belonging to separate bridging hydroxamates at distances of 2.066 Å (N7(H7A)···O20) and 1.891 Å (O20(H20A)···O1), respectively. The two crystallographically unique ClO_4^- counter ions show entirely different behaviour, with the first (labelled Cl1) sitting in between the two unique $\{Cu_5\}$ units in **7**, locked in place by numerous H-bonding interactions via its oxygen atoms (i.e. C16(H16B)···O12 = 2.507 Å, N5(H5B)···O13 = 2.557 Å and C12(H12)…O15 = 2.685 Å). The second counter anion (along with its symmetry equivalent) sits directly above one of the unique $\{Cu_5\}$ moieties (labelled Cu4-6), forming close contacts to Cu4 (Cu4-O17 = 2.646 Å) and Cu6 (Cu4-O16 = 2.504 Å). The $[Cu_5]$ moieties in **7** pack in columns along the *a* cell direction and these stacks then arrange themselves into the space efficient brickwork motif.

On close inspection of complexes **1** to **7** we notice that the position of their perchlorate counter anions varies significantly in relation to metallacrown proximity. Their weak coordination ability means that they will frequently reside at the periphery of a crystal and this is indeed the case in **1**, **3** and **4**. However, the structures in **2** and **5** show the perchlorates to reside above and below their $\{Cu_5\}$ moieties, forming weak close contacts to nearby Cu(II) ions along with numerous hydrogen bonds with juxtaposed metal bound ligands (i.e. -NMe_2 protons in **2**; MeOH and pyridinyl protons in **5**). Interestingly the structure in **7**, having two $\{Cu_5\}$ units in the asymmetric unit, shows one of the two crystallographically unique ClO_4^- anions to be weakly coordinating to one metallacrown while the other is held away from the first coordination sphere of the second $[Cu_5]$ unit. This observation highlights how the solvent ligands in **1**-**7** are able to move the anions inside or outside the metallacycle, depending on the H-bonding and coordination ability of the methanol or pyridine ligands involved.

Solution studies

Solid state IR spectroscopy on complexes **1**-**7** each gave peaks at ~ 1590 cm^{-1}, 1550 cm^{-1} and 1100 cm^{-1} which are characteristic for the hydroxamate C-O, C-N and N-O stretching modes, respectively.[15] The solution behaviour of metallacrowns **1**, **2** and **4** was analysed using mass spectrometry and UV-vis spectrophotometry. The electrospray mass spectra (TOF-ES+) obtained from **1**, **2** and **4** in H_2O / MeCN (50:50) solutions each exhibit two prominent peaks at *m/z* = 515 and 1129 corresponding to the $[Cu_5(L_1)_4]^{2+}$ and $[\{Cu_5(L_1)_4\} + \{ClO_4\}]^+$ species, respectively (Fig. 9 and ESI). Very small peaks (< 2%) at *m/z* = 1554 are also observed in certain cases (**1** and **4**) and may be tentatively attributed to the $[\{Cu_5(L_1)_4(MeCN)_8\} + \{ClO_4\}]^+$ species, whereby many of the remaining Cu(II) coordination sites are occupied by MeCN ligands originating from the analyte.

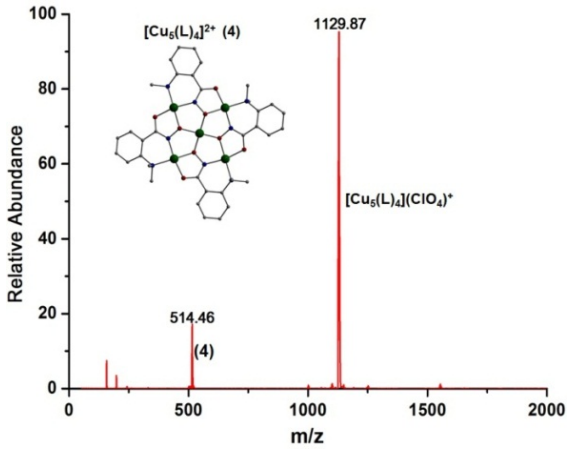

Figure 9 TOF-MS-ES+ spectrum of complex **4** in an H_2O/MeCN solvent matrix. The peaks at *m/z* = 514.46 and 1129.87 correspond to the $[Cu_5(L_1)_4]^{2+}$ and $[\{Cu_5(L_1)_4\} + \{ClO_4\}]^+$ species, respectively.

UV-vis spectra were obtained from methanolic solutions of L_1H_2, 4,4'-bipyridine and complexes **1** and **4** (see Figures S7-S11 for spectra). The spectrum in **1** shows absorptions at 230 and 273 nm and are attributed to the presence of π→π* transitions as corroborated on analysis of the L_1H_2 ligand in solution.[15] Likewise the spectra obtained from **4** exhibit absorptions at 234 and 267 nm (shoulder) and are attributed to π→π* transitions. Indeed the shoulder at 267 nm may be attributed to both the metal bound hydroxamate moieties and uncoordinated 4,4'-bipyridine ligands (due to its disassociation in solution), resulting in the reformation of the $[Cu_5(L_1)_4(MeOH)_4]^{2+}$ adduct (*i.e.* complex **1**). No significant changes were observed when **1** and **4** were measured in MeCN (Fig. S11). The solution stability of the $\{Cu_5(L_1)_4\}^{2+}$ cores in **1** and **4** became apparent when the same solutions were re-measured after one week to give duplicitous spectra. Indeed the solution stability of similar species has been observed previously.[16] The apparent low concentration solubility of the 2D extended architecture in **4** is attributed to the rather long and weak Cu-$N_{4,4'\text{-bipy}}$ bonds that are exhibited between the $\{Cu_5\}$ units and the 4,4'-bipyridine linker ligands. As expected, Uv-vis studies on the discrete cluster $[Cu_5(L_2)_4(MeOH)_4](ClO_4)_2.H_2O$ (**7**) and the 1D net $\{[Cu_5(L_2)_4(pz)_2(MeOH)_3](ClO_4)_2.MeOH\}_n$ (**6**) give similar spectra to those of **1** and **4** as shown in Figure S12.

Magnetic susceptibility studies

Dc magnetic susceptibility measurements were performed on powdered microcrystalline samples of **1**, **4** and **6** in the 300 – 5 K temperature range in an applied field of 0.1 T. The room temperature $\chi_M T$ values of 0.71 (**1**), 1.42 (**4**) and 1.22 (**6**) cm^3 K mol^{-1} are well below the spin-only value of ~1.88 cm^3 K mol^{-1} expected for five non-interacting Cu(II) ions, assuming g = 2.0. Complex **1** shows a steady decrease in its χ_MT product upon lowering temperature, reaching a minimum of ~0.42 cm^3 K mol^{-1} at 60 K before increasing slightly to a plateau of 0.44 cm^3 K mol^{-1}. The shapes of the curves for complexes **4** and **6** are somewhat similar in nature, a rapid decrease in the χ_MT product with decreasing temperature, with a plateau in the lower temperature region. Such behaviour is indicative of the presence of strong intramolecular antiferromagnetic exchange between the Cu(II) ions in all three $[Cu_5]$ species. The crystal structures in **1**, **4** and **6** show that there are two separate magnetic exchange pathways between the constituent Cu(II) centres. As shown in Figure 10 (inset), the J_1 parameter represents the $Cu(II)_{outer}$-$Cu(II)_{outer}$ pathway which comprises one Cu-N-O-Cu bridge (angles range from 160.46-177.04°), while J_2 describes exchange between the $Cu(II)_{outer}$-$Cu(II)_{inner}$ ions which are composed of one Cu-N-O-Cu pathway (angles range from 21.25-48.16°) and one Cu-O_{oxime}-Cu bridge (angles ranging from 113.47-121.56°).

For the interpretation of the magnetic properties of **1**, **4** and **6** we employed the model given in the inset of Figure 10 and the following isotropic spin-Hamiltonian:

$$\hat{H} = -2J_1(\hat{S}_1 \cdot \hat{S}_2 + \hat{S}_2 \cdot \hat{S}_3 + \hat{S}_3 \cdot \hat{S}_4 + \hat{S}_4 \cdot \hat{S}_1) - 2J_2(\hat{S}_1 \cdot \hat{S}_5 + \hat{S}_2 \cdot \hat{S}_5 + \hat{S}_3 \cdot \hat{S}_5 + \hat{S}_4 \cdot \hat{S}_5) + \sum_{i=1-5}\{\mu_B B g \hat{S}_i\}$$

The best-fit parameters obtained for **1** and **4** (keeping g fixed at 2.15) were J_1 = -139.77 cm^{-1}, J_2 = -295.31 cm^{-1} (**1**) and J_1 = -48.81 cm^{-1}, J_2 = -85.68 cm^{-1} (**4**). Fitting of the data for the 1D net (**6**) required the introduction of a Curie-Weiss parameter (θ) to account for intermolecular exchange through the axial pyrazine connector ligands (*via* the filled d_{z^2} orbital). The resultant best-fit parameters were J_1 = -86.04 cm^{-1}, J_2 = -145.15 cm^{-1} and θ = -0.23 K (with g fixed at 2.15). The J-values obtained are in line with those observed in other similarly bridged Cu(II) cages[8a] and give rise to an isolated S = ½ ground spin state in all cases.

The differences in the obtained J-values between complexes **1**, **4** and **6** can be ascribed to the significant structural discrepancies (changes in bond angles and lengths *etc*) and possibly to the additional electronic effects of the different axial ligands (i.e. MeOH in **1**, 4,4-bipyridine in **4** and pyrazine in **6**).

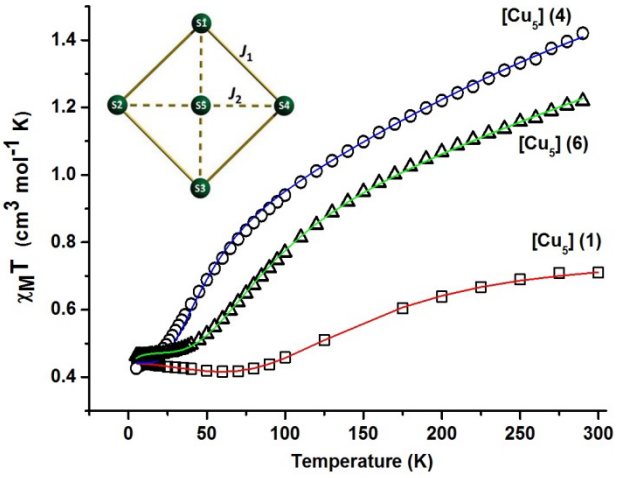

Figure 10 Plots of χ_MT vs. T for complex **1** (□), **4** (O) and **6** (Δ). The solid

lines are fits of the experimental data with spin-Hamiltonian (1) employing the schematic model in the inset. See text for details.

Conclusions

The ligands 2-(dimethylamino)phenylhydroxamic acid (L_1H_2) and 2-(amino)phenylhydroxamic acid (L_2H_2) have been successfully utilised in the synthesis of a family of 12-$MC_{Cu(II)}$-4 metallacrowns. N-donor ligands can be progressively added the the vacant axial sites on the Cu(II) ions in the planar $\{Cu_5\}$ core, exploiting both their coordinatively unsaturated nature and the ease of alcohol substitution, resulting in the formation of both discrete $[Cu_5]$ complexes (e.g. $[Cu_5(L_1)_4(py)_2](ClO_4)_2.py$ (**2**) and $[Cu_5(L_1)_4(py)_6](ClO_4)_2$ (**3**)) and 1D and 2D extended architectures, **4**-**6**. MS-ES+ and UV-vis studies each show solution stability with respect to their $\{Cu_5(L)_4\}^{2+}$ units which is highlighted by our ability to manipulate these moieties in solution, resulting in the construction of the extended architectures in **4**, **5** and **6**. Magnetic susceptibility measurements confirmed strong antiferromagnetic exchange between the Cu(II) ions in the $\{Cu_5\}$ core resulting in isolated S = ½ ground spin states.

Experimental Section

Infra-red spectra were recorded on a Perkin Elmer FT-IR *Spectrum One* spectrometer equipped with a Universal ATR Sampling accessory (NUI Galway). UV-visible studies were carried out on a Cary *100 Scan* (Varian) spectrophotometer. All spectra were normalised to unity once ε value calculations were completed. Elemental analysis were carried out at the School of Chemistry microanalysis service at NUI Galway. Variable-temperature, solid-state direct current (*dc*) magnetic susceptibility data down to 1.8 K were collected on a Quantum Design MPMS-XL SQUID magnetometer equipped with a 7 T *dc* magnet. Diamagnetic corrections were applied to the observed paramagnetic susceptibilities using Pascal's constants. TOF-MS-ES was carried out using a Waters LCT Premier XE system coupled with a Waters E2795 separations module.

Crystal structure information

The structures of **1**-**7** were collected on an Xcalibur S single crystal diffractometer (Oxford Diffraction) using an enhanced Mo source. Each data reduction was carried out on the CrysAlisPro software package. The structures were solved by direct methods (SHELXS-97)[17] and refined by full matrix least squares using SHELXL-97.[18] SHELX operations were automated using the OSCAIL software package.[19] All hydrogen atoms in **1**-**7** were assigned to calculated positions. All non-hydrogen atoms were refined anisotropic except for the MeOH (C21 and O20) and H_2O (O21) molecules of crystallisation in **7**. This H_2O molecule was modelled as disordered over three sites (labelled O21A-C). The pyridine molecule of crystallisation in **2** was restrained using the FLAT command.

Syntheses

All reactions were performed under aerobic conditions and all reagents and solvents were used as purchased. *Caution*: *Although no problems were encountered in this work, care should be taken when manipulating the potentially explosive perchlorate salts*. 2-(dimethylamino)phenylhydroxamic acid (L_1H_2) and 2-(amino)phenylhydroxamic acid (L_2H_2) were synthesised using a previously reported synthetic procedures.[4]

$[Cu_5(L_1)_4(MeOH)_4](ClO_4)_2$ (1): $Cu(ClO_4)_2{\cdot}6H_2O$ (0.25 g, 0.68 mmol), L_1H_2 (0.12 g, 0.68 mmol) and NaOH (0.027 g, 0.68 mmol) were dissolved in 40 cm^3 of MeOH and stirred for 16 h. The resultant green solution was filtered and X-ray quality crystals of **1** were obtained upon slow evaporation of the mother liquor. **1** was then collected and air dried with a yield of approximately 10%. Elemental analysis calculated (%) for: $C_{40}H_{56}Cl_2N_8O_{20}Cu_5$: C 35.39, H 4.16, N 8.25. Found (%): C 35.52, H 4.22, N 8.03. FT-IR (cm^{-1}): 3503(w), 2926(w), 1627(w), 1590(s), 1553(s), 1468(m), 1377(s), 1279(w), 1247(w), 1164(w), 1147(m), 1068(s), 1030(s), 1004(m), 955.17(m), 936(m), 905(s), 789(m), 775(m), 757(m), 708(m), 690(s), 663(s). UV/vis (MeOH): λ_{max} [nm] (ε_{max} 10^3 dm^3 mol^{-1} cm^{-1}): 207 (410), 271 (171.2). TOF MS-ES (%) m/z: 514.5 (100, $[Cu(II)_5(L_1)_4]^{2+}$), 1129.9 (44, $[\{Cu(II)_5(L_1)_4\} + \{ClO_4\}]^+$).

$[Cu_5(L_1)_4(py)_3](ClO_4)_2{\cdot}py$ (2): $Cu(ClO_4)_2{\cdot}6H_2O$ (0.25 g, 0.68 mmol), L_1H_2 (0.12 g, 0.68 mmol) and NaOH (0.027 g, 0.68 mmol) were dissolved in 40 cm^3 of MeOH and stirred magnetically. After 5 minutes 1 cm^3 (12.4 mmol) of pyridine was added and the solution was left to stir for a further 16 h. The resultant green solution was left to slowly evaporate resulting in the formation of X-ray quality crystals of **2** in ~15% yield. The crystals were then collected and air dried. Elemental Analysis calculated (%) for: $C_{51}H_{55}Cl_2N_{11}O_{16}Cu_5$: C 41.76, H 3.78, N 10.50. Found (%): C 42.01, H 3.95, N 10.68. FT-IR (cm^{-1}): 3515(w), 1616(w), 1587(m), 1539(m), 1489(w), 1469(m), 1445(w), 1411(m), 1381(m), 1289(w), 1221(w), 1150(w), 1087(s), 1032(m), 955(m), 930(m), 910(m), 820(m), 772(m), 709(m), 691(m), 670(m). TOF MS-ES (%) m/z: 514.5 (100, $[Cu(II)_5(L_1)_4]^{2+}$), 1129.9 (55, $[\{Cu(II)_5(L_1)_4\} + \{ClO_4\}]^+$).

$[Cu_5(L_1)_4(py)_6](ClO_4)_2$ (3): $Cu(ClO_4)_2{\cdot}6H_2O$ (0.25 g, 0.68 mmol), L_1H_2 (0.12 g, 0.68 mmol) and NaOH (0.027 g, 0.68 mmol) were dissolved in 40 cm^3 of MeOH. After 5 minutes of stirring 5 cm^3 (62.0 mmol) of pyridine was added and the solution left to stir for a further 16 h. Upon filtration and slow evaporation of the mother liquor X-ray quality crystals of **3** formed in ~10% yield. Elemental analysis calculated (%) for: $C_{66}H_{70}Cl_2N_{14}O_{16}Cu_5$: C 46.52, H 4.14, N 11.51. Found: C 46.41, H 4.33, N 11.26. FT-IR (cm^{-1}): 3519(w), 1612(w), 1591(m), 1539(m), 1492(w), 1465(m), 1446(w), 1408(m), 1380(m), 1285(w), 1220(w), 1150(w), 1087(s), 1031(m), 957(m), 934(m), 912(m), 815(m), 775(m), 705(m), 692(m), 669(m).

$\{[Cu_5(L_1)_4(4,4'\text{-bipy})_3](ClO_4)_2(H_2O)\}_n$ (4): $Cu(ClO_4)_2{\cdot}6H_2O$ (0.025 g, 0.068 mmol), L_1H_2 (0.012 g, 0.068 mmol) and NaOH (0.003 g, 0.075 mmol) were dissolved in 10 cm^3 of MeOH and

stirred for 4 h. The green solution obtained was filtered and layered with a MeOH solution (2 cm^3) of 4,4'-bipyridine (0.011 g, 0.068 mmol). Upon slow evaporation X-ray quality crystals of **4** were produced in a yield of ~15%. Elemental analysis calculated (%) for: $C_{66}H_{64}Cl_2N_{14}O_{17}Cu_5$: C 46.25, H 3.76, N 11.44. Found (%): C 46.39, H 3.30, N 11.58. FT-IR (cm^{-1}): 3514(w), 1617(w), 1588(m), 1537(m), 1490(w), 1468(m), 1447(w), 1410(m), 1383(m), 1288(w), 1222(w), 1149(w), 1085(s), 1033(m), 956(m), 933(m), 911(m), 817(m), 774(m), 706(m), 692(m), 668(m). UV/vis (MeOH): λ_{max} [nm] (ε_{max} 10^3 dm^3 mol^{-1} cm^{-1}): 234 (89.8), 267(sh), 360(broad-shoulder). TOF MS-ES (%) m/z: 514.4 (17, $[Cu(II)_5(L_1)_4]^{2+}$), 1129.9 (100, $[\{Cu(II)_5(L_1)_4\} + \{ClO_4\}]^+$).

$\{[Cu_5(L_1)_4(4,4\text{-azp})_2(MeOH)_2].(ClO_4)_2\}_n$ (5)

$Cu(ClO_4)_2{\cdot}6H_2O$ (0.1 g, 0.027 mmol), L_1H_2 (0.048 g, 0.027 mmol), NaOH (0.011 g, 0.027 mmol) and 4,4-azopyridine (0.05 g, 0.027 mmol) were dissolved in 20cm^3 of MeOH and stirred for 4h. Upon filtration and slow evaporation X-ray quality crystals of **5** were collected and air dried giving a yield of approximately 12%. Elemental analysis calculated (%) as $\{[Cu_5(L_1)_4(4,4\text{-azp})_2(MeOH)](ClO_4)_2{\cdot}3H_2O\}_n$ ($C_{47}H_{58}N_{12}O_{20}Cl_2Cu_5$): C 37.64, H 3.90, N 11.21. Found (%): C 37.15, H 3.41, N 10.74. FT-IR (cm^{-1}): 3518(w), 3028(w), 2936(w), 1589(s), 1552(s), 1489(w), 1470(m), 1412(m), 1372(s), 1282(w), 1254(w), 1227(w), 1150(w), 1087(s), 1043(s), 1025(s), 1014(s), 959(m), 938(m), 909(s), 876(m), 844(m), 775(s), 761(m), 712(m), 692(m), 658(m).

$\{[Cu_5(L_2)_4(pz)_2(MeOH)_3](ClO_4)_2{\cdot}MeOH\}_n$ (6): $Cu(ClO_4)_2{\cdot}6H_2O$ (0.100 g, 0.27 mmol), L_2H_2 (0.041 g, 0.27 mmol), NaOH (0.011 g, 0.27 mmol) and pyrazine (0.022 g, 0.27 mmol) were dissolved in 20 cm^3 MeOH and stirred for 2 hrs. The resultant green solution was then filtered and X-ray quality crystals of **6** were obtained in a yield of ~12% upon slow evaporation of the mother liquor. Elemental analysis calculated (%) as $\{[Cu_5(L_2)_4(pz)_2](ClO_4)_2{\cdot}4H_2O\}_n$ ($C_{36}H_{40}N_{12}O_{20}Cl_2Cu_5$): C 32.04, H 2.99, N 12.46. Found (%): C 31.86, H 2.59, N 12.34. FT-IR (cm^{-1}): 3209(w), 1597(m), 1563(m), 1542(s), 1495(m), 1417(m), 1381(s), 1307(w), 1288(w), 1088(s), 1030(s), 949(s), 871(w), 825(w), 783(m), 771(m), 747(s), 696(w), 681(m). UV/vis (MeOH): λ_{max} [nm] (ε_{max} 10^3 dm^3 mol^{-1} cm^{-1}): 260 (73.1), 360(sh).

$[Cu_5(L_2)_4(MeOH)_4](ClO_4)_2{\cdot}H_2O$ (7): $Cu(ClO_4)_2{\cdot}6H_2O$ (0.25 g, 0.68 mmol), L_2H_2 (0.102 g, 0.68 mmol) and NaOH (0.027 g, 0.75 mmol) were dissolved in 30 cm^3 MeOH and stirred for 3 hrs. The resultant green solution was filtered and allowed to stand. X-ray quality crystals of **7** were obtained upon slow evaporation of the mother liquid in ~10% yield. Elemental analysis calculated (%) for $C_{32}H_{40}N_8O_{21}Cl_2Cu_5$ (loss of three MeOH ligands): C 29.84, H 2.59, N 9.60. Found (%): C 29.39, H 2.28, N 9.61. FT–IR (cm^{-1}): 3422 (b), 3299 (w), 3229 (m), 2160 (w), 1980 (w), 1611 (w), 1596 (m), 1566 (s), 1536 (s), 1496 (m), 1445 (w), 1389 (m), 1372 (m), 1314(w), 1292(w), 1067(s), 960(m), 925(m), 825(w), 777(s), 747(s), 709(w), 683(m). UV/vis (MeOH): λ_{max} [nm] (ε_{max} 10^3 dm^3 mol^{-1} cm^{-1}): 265 (61.3), 375(sh).

Notes and references

[a] *School of Chemistry, NUI Galway, University Road, Galway, Ireland. Tel: +353-091-49-3462; E-mail: leigh.jones@nuigalway.ie.*

[b] *Department of Basic Medical Sciences, Royal College of Surgeons in Ireland, Medical University of Bahrain, Building No. 2441, Road 2835, Busaiteen 228, PO Box 15503. Adliya, Kingdom of Bahrain, Tel: +973-17-351450-2300; E-mail: dgaynor@rcsi-mub.com*

[c] *School of Chemistry, Joseph Black Building, University of Edinburgh, West Mains Road, Edinburgh, UK, EH9 3JJ.*

† Electronic Supplementary Information (ESI) available. See DOI: 10.1039/b000000x/. For crystal structure data for complexes **1- 7** see CCDC 885549-885552 (**1-4**) and 936487-936489 (**5-7**).

‡ Celebrating 300 years of Chemistry in Edinburgh.

1. (a) M. Paris, M. Porcelloni, M. Binaschi and D. Fattori, *J. Med. Chem.*, 2008, **51**, 1505. (b) Z. Amtul, R. Atta ur, R. A. Siddiqui and M. I. Choudhary, *Curr. Med. Chem.*, 2002, **9**, 1323-1348. (c) D. T. Puerta and S. M. Cohen, *Curr. Top. Med. Chem.*, 2004, **4**, 1551.
2. (a) E. M. F. Muri, M. J. Nieto, R. D. Sindelar and J. S. Williamson, *Curr. Med. Chem.,* 2002, **9**, 1631-1653. (b) C. J. Marmion, D. Griffith and K. B. Nolan, *Eur. J . Inorg. Chem.*, 2004, **2004**, 3003.
3. D. Gaynor, Z. A. Starikova, S. Ostrovsky, W. Haase and K. B. Nolan. *Chem. Commun*., 2002, 506.
4. D. Gaynor, Z. A. Starikova, W. Haase and K. B. Nolan. *Dalton Trans*., 2001, 1578.
5. (a) G. Mezei, C. M. Zaleski and V. L. Pecoraro. *Chem. Rev.,* 2007, **107**, 4933. (b) I. A. Golenya, E. Gumienna-Kontecka, A. N. Boyko, M. Haukka and I. G. Fritsky. *Inorg. Chem.,* 2012, **51(11)**, 6221.
6. (a) G. A. Ardizzoia, S. Cenini, G. La Monica, N. Masciocchi and M. Moret. *Inorg. Chem.,* 1994, **33**, 1458. (b) A. Maspero, S. Brenna, S. Galli and A. Penoni. *J Organomet. Chem*. 2003, **672**, 123. (c) M. Yoshizawa, J. K. Klosterman and M. Fujita, *Angewandte Chemie-International Edition*, 2009, **48**, 3418.
7. R. H. Fish. *Coord. Chem. Rev.,* 1999, **185-186**, 569.
8. (a) A. V. Pavlishchuk, S. V. Kolotilov, M. Zeller, L. K. Thompson, I. O. Fritsky, A. W. Addison and A. D. Hunter. *Eur. J. Inorg. Chem*., 2010, 4851. (b) A. V. Pavlishchuk, S. V. Kolotilov, M. Zeller, O. V. Shvets, I. O. Fritsky, S. E. Lofland, A. W. Addison and A. D. Hunter., *Eur. J. Inorg. Chem*., 2011, 4826.
9. J. Jankolovits, C. M. Andolina, J. W. Kampf, K. N. Raymond and V. L. Pecoraro. *Angew. Chem. Int .Ed.,* 2011, **50**, 1.
10. (a) R. W. Saalfrank, A. Scheürer, I. Bernt, F. W. Heinemann, A. V. Postnikov, V. Schunemann, A. X. Trautwein, M. S. Alam, H. Rupp and P. Müller. *Dalton Trans.,* 2006, 2865. (b) S. Osa, T. Kido, N. Matsumoto, N. Re, A. Pochaba and J. Mrozinski. *J. Am. Chem. Soc*., 2004, **126**, 420. (c) T. T. Boron, J. W. Kampf and V. L . Pecoraro. *Inorg. Chem.,* 2010, **49(20)**, 9104.
11. A. W. Addison, T. N. Rao, J. Reedjik, J. van Rijn and G. C. Verschoor. *J. Chem. Soc. Dalton Trans.,* 1984, 1349.
12. S. H. Seda, J. Janczak and J. Lisowsky. *Inorg. Chim. Acta.* 2006, **359(4)**, 1055.
13. (a) J. J. Bodwin and V. L. Pecoraro., *Inorg. Chem*., 2000, **39**, 3434. (b) A. B. Lago, J. Pasán, L. Cañadillas-Delgado, O. Fabelo, F. J. M. Casado, M. Julve, F. Lloret and C. Ruiz-Pérez. *New. J. Chem*., 2011, **35**, 1817.
14. (a) M. Moon, I. Kim and M. Soo Lah. *Inorg. Chem*., 2000, **39**, 2710. (b) R. Wang, M. Hong, J. Luo, R. Cao and J. Wang. *Chem. Commun*., 2003, 1018.
15. (a) D. H. Williams and I. Fleming. *Spectroscopic Methods in Organic Chemistry*. McGraw Hill (5th Ed.). 1995. (b) D. A. Brown and A. L. Roche. *Inorg. Chem*., 1983, **22**, 2199.
16. (a) B. R. Gibney, D. P. Kessissoglou, J. W. Kampf and V. L. Pecoraro. *Inorg. Chem*., 1994, **33(22),** 4840. (b) M. Careri, F. Dallavalle, M. Tegoni and I. Zagnoni, *Journal of Inorganic Biochemistry*, 2003, **93**, 174. (c) D. Bacco, V. Bertolasi, D. Dallavalle, L. Galliere, N. Marchetti, L. Marchio, M. Remelli and M. Tegoni. *Dalton Trans.,* 2011, **40**, 2491.

17. G. M. Sheldrick, *Acta. Crystallogr., Sect. A: Found. Crystallogr*., 1990, A46, 467.
18. G. M. Sheldrick, SHELXL-97, A computer programme for crystal structure determination, University of Gottingen, 1997.
19. P. McArdle, P. Daly and D. Cunningham, *J. Appl. Crystallogr.,* 2002, 35, 378.

We present a family of 12-$MC_{Cu(II)}$-4 [Cu_5] metallacrowns whose terminal solvent ligands may be exchanged in a controlled and progressive manner ultimately towards the self-assembly of 1- and 2D extended networks, depending on the nature of the ditopic connector ligand introduced.